Vision Research 154 (2019) 1–13

Contents lists available at ScienceDirect

Vision Research

journal homepage: www.elsevier.com/locate/visres

# Phase-selective masking with radial frequency contours

Michael Slugocki[a,*], Allison B. Sekuler[b,c,a], Patrick J. Bennett[a]

[a] Department of Psychology, Neuroscience and Behaviour, McMaster University, Hamilton, Ontario, Canada
[b] Rotman Research Institute, Baycrest Health Sciences, Toronto, Ontario, Canada
[c] Department of Psychology, University of Toronto, Toronto, Ontario, Canada

ARTICLE INFO

*Keywords:*
Radial frequency contours
Shape perception
Lateral masking

ABSTRACT

Sensitivity to changes in the shape of a closed-contour figure is affected by surrounding figures (Vision Research 44 (2004) 2815–2823). We examined how between-contour masking depends on radial frequency. Experiment 1 replicated previous studies that found that masking between adjacent radial frequency (RF) patterns was greatest when the two shapes were phase aligned, and that the magnitude of masking declined approximately linearly with increasing phase offsets. In addition, we found that the effect of phase offset on masking was very similar for RFs ranging from 3 to 8, a result that suggests that sensitivity to phase decreases with increasing radial frequency. Experiment 2 tested this idea and found that phase discrimination threshold for single cycles of curvature was approximately proportional to radial frequency. Experiment 3 showed that both curvature maxima and minima contribute to phase dependent masking between RF contours. Together, Experiments 1–3 demonstrate that the strength of phase-dependent masking does not depend on RF, but is related to sensitivity for phase shifts in isolated contours, and is affected by both positive and negative curvature extrema. We discuss these results in relation to properties of curvature sensitive neurons.

## 1. Experiment 1

The perception of global shape of closed-contour figures relies on the extraction and integration of local contour features to represent larger curvature elements (Altmann, Bülthoff, & Kourtzi, 2003; Geisler, Perry, Super, & Gallogly, 2001; Wang & Hess, 2005). Prior research has used Radial Frequency (RF) contours to study how the human visual system detects, extracts, and integrates curvature information to represent shape (Bell & Badcock, 2009; Bell, Wilkinson, Wilson, Loffler, & Badcock, 2009; Day & Loffler, 2009; Hess, Wang, & Dakin, 1999; Jeffrey, Wang, & Birch, 2002; Kurki, Saarinen, & Hyvarinen, 2014; Loffler, Wilson, & Wilkinson, 2003; Wilkinson, Wilson, & Habak, 1998). By modulating the radius of a circle in polar coordinates, RF contours can represent a variety of increasingly complex shapes while allowing researchers to control important stimulus parameters (Wilson & Wilkinson, 2002; Wilson, Wilkinson, Lin, & Castillo, 2000). Much research has focused on the detection of RF contours in isolation, but less attention has been devoted towards studying spatio-temporal interactions between contours. Because local features affect detection thresholds of other unrelated objects within naturalistic images (Alam, Vilankar, Field, & Chandler, 2014), studying the local and global interactions between shapes presumably is needed to better understand how the human visual system processes form in naturalistic contexts.

Previous work investigating spatial interactions between shapes defined by RF contours has demonstrated that these interactions depend on the rotational phase alignment between a mask and target stimulus (Habak, Wilkinson, & Wilson, 2009; Habak, Wilkinson, & Wilson, 2006; Habak, Wilkinson, Zakher, & Wilson, 2004). When the points of maximum curvature are aligned between RF contours (i.e., zero-phase difference), thresholds for detecting RF curvature are significantly elevated relative to a baseline condition that contains no masking stimulus, and the strength of masking diminishes as the relative phase difference increases between the mask and target RF contours (Habak et al., 2009; Habak et al., 2006; Habak et al., 2004). These results are consistent with behavioural models that suggest shapes are discriminated using points of maximum orientation difference from circularity (i.e., curvature maxima) along a contour (Dickinson, Bell, & Badcock, 2013; Dickinson, Cribb, Riddell, & Badcock, 2015; Dickinson, Haley, Bowden, & Badcock, 2018), as offsets in spatial alignment of curvature maxima between two RF contours results in less masking. However, it is unclear how this relation between masking and phase alignment depends on the radial frequencies of the mask and target contours. Given that sensitivity to changes in curvature depends on radial frequency, and that low and high RF patters appear to be processed by different mechanisms (Loffler et al., 2003; Schmidtmann, Kennedy, Orbach, & Loffler, 2012), it is reasonable to suspect that

* Corresponding author.
*E-mail addresses:* slugocm@mcmaster.ca (M. Slugocki), sekuler@mcmaster.ca (A.B. Sekuler), bennett@mcmaster.ca (P.J. Bennett).

https://doi.org/10.1016/j.visres.2018.10.013
Received 21 June 2018; Received in revised form 18 October 2018; Accepted 18 October 2018
Available online 09 November 2018

phase-alignment masking would depend on the radial frequencies of the mask and target contours.

Previous studies suggest that summation of local curvature information along an RF contour depends on the frequency of curvature modulation (Loffler et al., 2003; Schmidtmann et al., 2012). For radial frequencies between 2 and 8 cycles/$2\pi$, detection thresholds improve with increasing number of modulation cycles at a rate that is greater than that predicted by probability summation (Hess et al., 1999; Loffler et al., 2003; Schmidtmann et al., 2012). Based on these results, summation of curvature along the contour of these shapes is thought to rely upon the integration of local information, possibly by a global shape mechanism (Hess et al., 1999; Loffler et al., 2003; Schmidtmann et al., 2012). However, it is important to note that the rate of curvature summation differs across RF contours between 2 and 8 cycles/$2\pi$, which suggests that a global integration is more efficient for some radial frequencies compared to others (Hess et al., 1999; Loffler et al., 2003; Schmidtmann et al., 2012). For high RF contours (i.e., >8cycles/$2\pi$), curvature summation is consistent with predictions of models that assume that the detection of curvature in extended contours is based on probability summation of local detectors (Hess et al., 1999; Loffler et al., 2003; Schmidtmann et al., 2012).

More recently, Baldwin, Schmidtmann, Kingdom, and Hess (2016) have questioned whether global pooling of local curvature is necessary to account for RF detection. By investigating RF detection under a Signal Detection Theory (SDT) framework rather than High Threshold Theory (HTT) as previous summation studies on RF detection have used, Baldwin et al. (2016) demonstrated that probability summation as a model describing the mechanism governing detection of RF contours cannot be rejected. Schmidtmann and Kingdom (2017) have extended this logic by developing a model that sufficiently accounts for curvature detection thresholds along both line and closed contour stimuli. A notable novelty in the model developed by Schmidtmann and Kingdom (2017) is the addition of a modulation transfer function for curvature frequency, which explains the flattening of detection thresholds to curvatures of intermediate and high frequencies, and aims to provide a unified theory for perception of curvature across contours.

Despite challenges to theories based on global summation of local curvature, this theory still remains plausible. Green, Dickinson, and Badcock (2017, 2018a, 2018b, 2018c) conducted a series of studies to examine how alterations to the original experimental design utilized by Baldwin et al. (2016) might influence the ability to distinguish between different theories of curvature summation across shapes. A key finding across these studies is that when phase of RF contours is randomized across trials, probability summation fails to predict performance across a wide range of experimental designs, even when assumptions of SDT are considered (Green et al., 2017, 2018a, 2018b, 2018c). This finding suggests curvature frequency (i.e., the number of visible cycles of curvature) and *phase* may jointly determine the strength of summation of curvature around closed contours (Green et al., 2017, 2018a, 2018b, 2018c).

Differences in the ability of shape mechanisms to integrate curvature along contours raises the possibility that the effect of phase alignment on masking may also vary as a function of radial frequency. Lateral interactions (i.e., masking) between RF contours are hypothesized to arise from the improper summation of curvature signals along target and mask contours at locations of peak curvature (Habak et al., 2004; Poirier & Wilson, 2006). As the phase offset between a target and mask increases, the probability that curvature signals are improperly integrated across regions of peak curvature declines because the phase shift changes the polar angle at which these curvature maxima occur. As a result, masking declines with increasing phase offset between shapes (Habak et al., 2004). Because summation of curvature signals depends on radial frequency and phase uncertainty, perhaps the phase-dependency of masking, thought to arise from improper summation of curvature signals at specific locations along a shape, also depends on radial frequency. This hypothesis predicts that shape interactions should operate over fixed distances, perhaps due to the fixed receptive field size of curvature sensitive neurons, which should cause the strength of masking to vary with changes in physical distance between curvature extrema, rather than phase. Therefore, the effect of phase on masking should depend on radial frequency. However, if phase-dependent interactions between shapes instead depend upon the similarity between representations of a target and mask, as might occur, for example, if both contours were represented with a radial modulation function, then phase dependency may be constant across RF contours. Such a result would suggest that the summation that contributes to phase-dependent masking, and the type of summation that contributes to the detection of curvature along a shape, likely occur at different stages of visual processing.

The aim of the current study therefore was to investigate how the radial frequency of contour curvature affects the rate at which masking declines as a function of the phase alignment between two shapes.

### 1.1. Methods

#### 1.1.1. Participants

One of the authors (MS) and eight naïve, experienced psychophysical observers participated in Experiment 1. Observer MS was tested in all conditions and the remaining observers were randomly assigned to one of four conditions, for a total of three observers per condition. The mean age of the observers was 20.8 years ($SD$ = 1.4) and all observers had normal or corrected-to-normal visual acuity. Experimental protocols were approved by the McMaster University Research Ethics Board, and consent of the participant was collected prior to the start of the experiment.

#### 1.1.2. Apparatus & stimuli

Stimuli were presented on a Sony Model GDM-F520 monitor (1024 × 768) with a refresh rate of 100 Hz and a mean luminance of 62.9 cd/m$^2$. An APPLE G4 2.66 GHz Quad-Core Intel Xeon computer generated and displayed the shapes using Matlab 10.7.0 (Mathworks Inc., Natick, MA) and the Psychophysics Toolbox (Brainard, 1997; Pelli, 1997). A chinrest was used to maintain a constant viewing distance of 131 cm. From this distance, a single pixel subtended 41.5 arc seconds.

Stimuli were comprised of RF contours generated by sinusoidally modulating the radius of a circle, and were defined by the equation (Wilkinson et al., 1998):

$$r(\theta) = \bar{r}(1 + Asin(\omega\theta + \phi)) \quad (1)$$

where $\theta$ is the angle in radians, $\bar{r}$ is the radius of the contour, $A$ is the amplitude of modulation expressed as a proportion of the radius of the circle, $\omega$ is the radial frequency in cycles per circumference (cy/$2\pi$), and $\phi$ is angular phase. The cross-sectional luminance profile of each contour was defined by a fourth derivative Gaussian [D4; see] (Wilkinson et al., 1998). All RF contours had a luminance contrast of 99% and a peak spatial frequency of 8 cpd. All target RF contours had a mean radius of 1.14°. Each RF mask was positioned outside the target RF contour, and the mean target-mask distance was 0.35°. The target and mask always had the same radial frequency, and masking was measured with four radial frequencies (RF3, RF5, RF6, or RF8; see

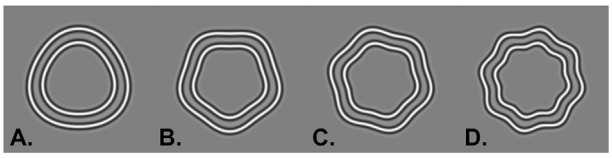


**Fig. 1.** Example of stimuli used in Experiment 1. Stimuli were comprised of RF contours, here shown at a relative target-mask phase of 0°, with a contrast at 99% contrast and a deformation amplitude of 5%. The frequency of angular modulation per circumference varied across conditions: (a) RF3 (b) RF5 (c) RF6 (d) RF8.


**Fig. 2.** Example of seven target-mask phase combinations (A-G: 0, 30, 60, 90, 120, 150, & 180 deg) used throughout the study for an RF5 contour. The amplitude of both the target and mask are presented here at suprathreshold values for purposes of illustration only.

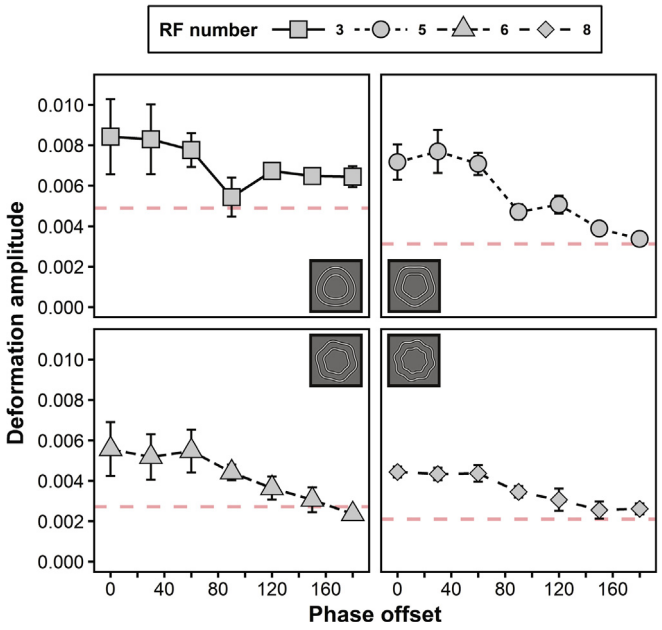


**Fig. 3.** Detection thresholds as a function of the target-mask phase offset across the four RF conditions. In general, as the phase offset between the target and mask increases, there is a decrease in the amplitude of modulation required to make a correct detection judgement. Baseline measures for each RF contour are represented by the horizontal dashed red line. Error bars represent ± 1 SEM.

Fig. 1). The modulation amplitude of each mask was set to 15 times the baseline detection threshold for that particular RF. The phase of the mask RF was always 0°, and thresholds were measured with seven target phases (0°, 30°, 60°, 90°, 120°, 150°, 180°). Examples of mask-target combinations are shown in Fig. 2. The four mask RFs and seven target-mask relative phases yielded a total of 28 masking conditions. For baseline, the phase of the target was varied across trials at three phase orientations 45°, 135°, 225°.

### 1.1.3. Procedure

Thresholds were measured with a two-alternative forced-choice paradigm and the method of constant stimuli. Each trial consisted of two stimulus intervals: one interval contained a circular contour (i.e., RF0), the other contained a target RF contour. Trials were initiated by observers by pressing the spacebar key on a computer keyboard. After a 300 ms interval a central fixation dot flickered for 500 ms and, after another 300 ms interval, two 150 ms stimulus intervals were presented with a 300 ms inter-stimulus-interval. The task was to select the stimulus interval that contained the target contour by pressing a key on a computer keyboard. No feedback was provided. The position of each contour on every trial was jittered within a 0.17° radius from the center of the screen; the mask and target were jittered in the same direction. Mean luminance remained constant throughout a testing session.

Prior to the start of the experiment, observers received three practice trials to familiarize themselves with the stimuli and task. Following practice, there was a 60 s light adaptation period, during which the observer fixated the center of the display. A single block of trials comprised either three or four target-mask phase combinations presented at seven different target modulation amplitudes, for a total of 504 or 672 trials per block, respectively. Each amplitude and phase combination was shown 24 times in a random order within a block. Each observer completed a block containing three different target-mask phase combinations (0°, 90°, 180°), and a block containing four different target-mask phase combinations (30°, 60°, 120°, 150°) within a single experimental session. The order in which observers completed blocks was randomized within a session, and across observers. We adopted this block design to give observers a short break between testing blocks, and do not believe this decision in design influenced the outcome of our experiment. All observers completed two sessions, with each session being run on a separate day. In general, participants completed both sessions across two consecutive days, with each session lasting approximately 1.5 h.

### 1.1.4. Results

All analyses were performed using the statistical computing software R (R Core Team, 2017). Data for each target-mask phase combination were fit using maximum likelihood estimation with a psychometric function defined as:

$$\psi(x;\alpha,\beta,\gamma,\lambda) = \gamma + (1-\gamma-\lambda)F_W(x;\alpha,\beta) \quad (2)$$

where $x$ is RF modulation amplitude, $\gamma$ and $\lambda$ set the upper and lower asymptotes, and $F_W(x;\alpha,\beta)$ is a Weibull function (Weibull, 1951) defined as:

$$F_W = 1 - \exp\left(-\left(\frac{x}{\alpha}\right)^{\beta}\right) \quad (3)$$

Threshold was defined as the RF modulation amplitude yielding 75% detection accuracy.

Thresholds were analyzed using a mixed linear model estimated with the lme4 package (Bates, Mächler, Bolker, & Walker, 2015). Degrees of freedom for the mixed model were approximated using the Kenward-Roger method (Kenward & Roger, 1997), which rescales the $F$ ratios in addition to adjusting the degrees of freedom to better approximate F-distributions for mixed linear models (Judd, Westfall, & Kenny, 2012). For brevity, we report only the $F$ tests from the linear mixed-effects regression analyses (i.e., the analysis of variance of Type III sums of squares with Kenward-Roger approximation for degrees of freedom). Post-hoc comparisons between masking conditions were performed using paired, two-sided $t$ tests with $p$ values adjusted with the Holm-Bonferonni method and familywise $\alpha = 0.05$ (Holm, 1979).

Fig. 3 displays RF detection thresholds averaged across all observers for each RF condition. For each radial frequency, threshold declined with increasing mask-target phase offset. In addition, close inspection of the figure indicates that detection thresholds decreased with increasing radial frequency. Finally, the effect of phase on threshold appeared to be very similar across RF conditions.

These set of observations were confirmed through the use of a mixed model, which was fitted with two fixed effects (RF condition and Phase) and one random effect (Observer). The ANOVA revealed significant main effects of RF condition ($F_{3,74.70} = 9.80$, $p < .0001$) and Phase ($F_{1,68.22} = 78.89$, $p < .0001$). The interaction between RF condition and Phase was not significant ($F_{3,68.22} = 2.45$, $p = .07$).

A more focused and potentially more powerful test of the RF × Phase interaction was conducted by calculating the linear and quadratic trends of threshold across phase offset (see Fig. 4). The linear trend was consistently below zero and approximately equal for all RF conditions, whereas the quadratic trend was near zero in all RF conditions. These analyses suggest that thresholds decreased approximately linearly with

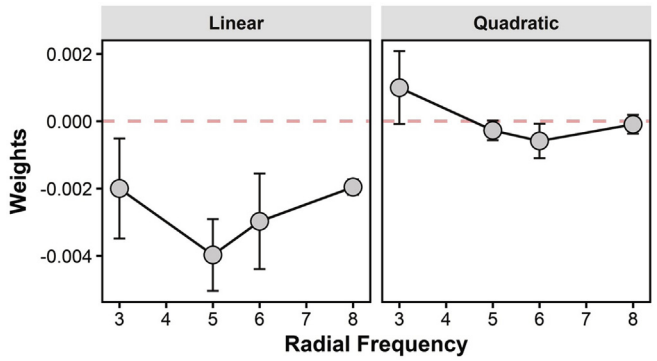


**Fig. 4.** Values of the linear and quadratic trends of curvature detection thresholds across phase offsets plotted as a function of radial frequency. Error bars represent ± 1 SEM.

phase offset at similar rates in all RF conditions.

### 1.2. Discussion

Results from Experiment 1 demonstrate a decline in thresholds with increasing RF, consistent with findings from previous studies (Dickinson, McGinty, Webster, & Badcock, 2012; Schmidtmann & Kingdom, 2017; Wilkinson et al., 1998). Furthermore, data from Experiment 1 show that phase alignment between target and mask contours affects the strength of masking. Lastly, the decline in threshold was approximately linear across phase offsets and the linear trend did not differ appreciably across RF conditions. These results are inconsistent with theories of masking between RF contours that hypothesize masking is caused by improper pooling of features across the receptive fields of curvature sensitive neurons (Habak et al., 2004; Habak et al., 2006; Habak et al., 2009; Poirier & Wilson, 2007). Because these theories predict that masking should vary with the physical distance between curvature extrema, the effect of phase on masking should vary as a function of radial frequency, as an equal change in phase results in different changes in absolute polar angle across RF contours (see Fig. 5). Furthermore, the constant effect of phase observed across RF conditions is surprising in light of previous work suggesting that curvature is summed differently along low- and high-frequency radial contours.

Perhaps current theories of masking between shapes cannot explain these findings because they do not take into consideration an observer's ability to detect relative phase shifts as a function of radial frequency. For example, the uniform effect of phase on RF masking is consistent with the idea that sensitivity to phase *per se* declines with increasing radial frequency. To our knowledge, the assumption that phase discriminability differs across RF contours has not been tested. Given its importance for explaining RF phase-dependent masking, Experiment 2 tested the assumption by measuring sensitivity for phase shifts of single-cycle RF contours as a function of radial frequency. Specifically, we predict that phase discrimination thresholds should be proportional to radial frequency.

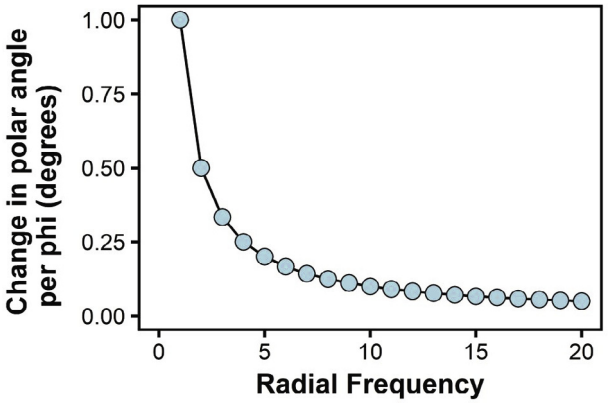


**Fig. 5.** Figure displays the absolute change in polar angle that results from a single degree change in phase ($\phi$) as a function of radial frequency. As radial frequency increases, changes in polar angle accompanying a shift in phase decline.

## 2. Experiment 2: does sensitivity to shifts in phase vary across radial frequencies?

Theories of masking between RF contours hypothesize that masking results from excess pooling of curvature features by curvature-sensitive neurons (Habak et al., 2004; Habak et al., 2006; Habak et al., 2009; Poirier & Wilson, 2007), possibly in V4 (Pasupathy & Connor, 2001; Pasupathy & Connor, 2002). These theories predict that sensitivity to shifts in phase may differ between RF contours as a consequence of the organization of receptive fields positioned radially from the origin of fixation. Because the range of polar angles over which a single cycle of modulation occurs is inversely related to radial frequency, neurons in V4 that respond to curvatures at different polar angles will produce responses that are more spatially dispersed for low RF contours, and more localized for high RF contours. Following a change in phase, which alters the polar angles of curvature features such as maxima and minima, RF contours that evoke dispersed responses may be more difficult to discriminate because the population response produced by V4 neurons will be similar across larger phase shifts compared to shapes that evoke highly localized responses. However, as mentioned in the Discussion section of Experiment 1, it is important to realize that the absolute change in polar angle produced by a constant phase shift decreases as radial frequency increases (see Fig. 5). In other words, shifting curvature features (e.g., curvature maxima) by a specific polar angle requires a larger phase shift at high RFs than low RFs. According to this line of reasoning, the similar results that we obtained across RFs (Fig. 3) implies that sensitivity to phase shifts of RF patterns *decreases* with radial frequency. Therefore, for the effect of phase offset between a target and mask to remain constant across RF contours, as was found in Experiment 1, the theories of RF contour masking outlined above must assume that sensitivity to phase shifts of single cycles of curvature decreases as a function of radial frequency. Specifically, we predict that phase discrimination thresholds should be proportional to radial frequency. To our knowledge, this assumption has not been tested. Given its importance for explaining RF phase-dependent masking, Experiment 2 tested the assumption by measuring sensitivity for phase shifts of single-cycle RF contours as a function of radial frequency.

### 2.1. Methods

#### 2.1.1. Participants

Five new naïve observers participated in Experiment 2. The mean age of the observers was 27.6 years ($SD$ = 1.9) and all observers had normal or corrected-to-normal visual acuity. Experimental protocols were approved by the McMaster University Research Ethics Board, and consent of the participant was collected prior to the start of the experiment.

#### 2.1.2. Apparatus & stimuli

The apparatus was the same as the one used in Experiment 1. The stimuli were single cycle contours defined by the equation adapted from Loffler et al. (2003)

$$r(\theta) = \bar{r}\left(1 + B\frac{\theta - \theta_c}{\sigma}e^{-(\theta-\theta_c)^2/\sigma^2}\right), \text{ for } \begin{matrix}\theta_c + \frac{2}{\omega}\pi \geqslant \theta > \theta_c \\ \theta_c - \frac{2}{\omega}\pi \leqslant \theta < \theta_c\end{matrix}$$
$$= \bar{r} \quad \text{elsewhere} \tag{4}$$

Parameters of the first derivative Gaussian, $B$ and $\sigma$, were


**Fig. 6.** Example of single cycle RF contours used in Experiment 2 to test for sensitivity to shifts in phase. The amplitude modulation of each cycle was set at 15× the baseline detection threshold for that RF condition for each observer. In total, three RF conditions were tested: (a) RF3 (b) RF5 (c) RF8 (d) RF11. The amplitude modulation of each cycle was set to 0.07 in this figure to make undulations readily noticeable, while in the experiment amplitude modulations never reached such large values. All patterns are shown at $\theta_c$ set to zero.

constrained to those values that best matched the maximum slope, and maximum and minimum deviation in amplitude of a single cycle of modulation as sampled from a full RF pattern (as defined in Eq. (1)). To ensure that each cycle was clearly visible to observers, the maximum and minimum amplitude of each cycle was set to 15× the baseline detection threshold obtained with single cycle patterns. The radial frequency of a single cycle depends on where the upper and lower bounds are defined in Eq. (4), which is determined by $\omega$. Parameters $\bar{r}$ and $\theta$ for these single cycle RF contours were identical to those used in Experiment 1. Angular phase of patterns was determined by $\theta_c$, which was defined by:

$$\theta_c = \frac{\phi}{\omega} \tag{5}$$

where $\phi$ represents the phase of the pattern as defined in Eq. 1. Therefore, $\phi$ changes the phase of a pattern by changing the value of $\theta_c$, as the value of $\omega$ remains fixed for a given a pattern. In total, four RF contours (defined by $\omega$) were tested: RF3, RF5, RF8 and RF11 (see Fig. 6).

#### 2.1.3. Procedure

Phase discrimination thresholds were measured with a two-interval forced choice procedure. On each trial, two shapes were flashed onscreen across two intervals: each interval had a 150 ms duration, and the inter-stimulus interval was 500 ms. The first shape had an initial starting position ($\theta_c$) set to a random value between 0 and $2\pi$. The second shape had a phase of $\phi + \delta_\phi$, where $\phi$ was the same pedestal phase as the first, and $\delta_\phi$ was a shift in phase. The observer's task was to determine if the second pattern was rotated clockwise or counterclockwise relative to the first pattern. The phase shift ($\delta_\phi$) was adjusted across trials with two independent, inter-leaved staircases. Both staircases followed a 2-down, 1-up rule, that terminated after 16 reversals, with final thresholds being defined by the average phase shift discriminated by observers of the last 8 reversals. The staircase step size started at 0.2 log units of phase shift from an initial starting value of 0.1066 radians (approximately 6.1 degrees), and was gradually reduced to a final step size of 0.02 log units following 2, 5, 8, and 11 reversals. On half the trials, the change in phase was positive, while on the remainder of trials it was negative. Observers completed 20 practice trials prior to the start of the experiment to ensure they understood the task. Each observer completed a minimum of 2 sessions per RF condition.

### 2.2. Results

The results from Experiment 2 are shown in Fig. 7. In every observer, phase shift thresholds were lowest for RF3 contours and increased monotonically with increasing radial frequency. Thresholds were analyzed with mixed linear models following the same procedures used in Experiment 2, with one fixed effect (RF condition) and two random effects (Observer and Session). The ANOVA revealed a significant effect of RF condition ($F_{3,7} = 15.22$, $p = .0018$). Post-hoc pairwise comparisons revealed significant differences between all RF conditions ($p_{Holm} < .01$) except between RF3 and RF5 conditions ($p_{Holm} = .05$) and between RF8 and RF11 conditions ($p_{Holm} = .15$).

To examine whether phase discrimination thresholds are proportional to radial frequency, we computed the best-fitting regression line for each subject, and then calculated the mean and median slope across linear fits. As can be seen in Table 1, the mean and median slope across observers was 2.82 and 2.42, respectively. Using the average values of the regression intercept and slope to calculate phase ($\phi$) discrimination thresholds for each RF ($\omega$), and Eq. 5 to convert phase to polar angle ($\theta_c$), we estimate that the just discriminable polar angle for our stimulus conditions was 3.07 deg.

### 2.3. Discussion

Experiment 2 found that sensitivity to shifts in phase for single cycles of curvature differ as a function of the radial frequency from which the cycles were sampled. It is unlikely that these results reflect an inability of observers to detect curvature deformations at different radial frequencies, as the amplitude of each RF contour was set to 15 times the curvature detection threshold in each condition.

Another possibility is that observers may have had greater trouble localizing the single RF cycle for high RF contours compared to low RF contours. Such differences in spatial uncertainty for RF location would make it difficult for observers to make comparisons of phase across stimulus intervals. Loffler et al. (2003) showed that, relative to phase randomized conditions, fixing the phase of single-cycle RF patterns lowered curvature detection thresholds for intermediate RF contours (RF5) compared to low (RF3) or high (RF24) patterns. These results suggest that at least for the detection of single-cycles of curvature, spatial uncertainty has a greater effect on performance for intermediate than for low or high RF contours. This non-monotonic effect differs from the linear relationship that we found between phase discrimination thresholds and RF, which suggests that spatial uncertainty is unlikely to be the primary reason why phase discrimination thresholds decline with increasing radial frequency. Of course it is not clear that the differences in spatial uncertainty across radial frequencies observed by Loffler et al. (2003) also extend to the stimulus conditions used here, in which RF amplitude was well above detection threshold. Therefore, it remains possible that the results in Fig. 7 may be due, at least in part, to the effects of spatial uncertainty.

A third possibility is that observers use absolute change in angular position of curvature maxima to detect changes in phase, much like observers use these points to discriminate between RF contours (Dickinson et al., 2013; Dickinson et al., 2015; Dickinson et al., 2018). In the context of phase discrimination, an observer could locate a point of maximum curvature, and track the change in position of that point regardless of the curvature occupying the remainder of the contour. This explanation accurately accounts for our results, but does not explain the neural mechanism being used to encode shape. Therefore, we also propose that this encoding scheme reflects the organization and size of curvature sensitive cells in V4 (Habak et al., 2004; Habak et al., 2009). The overlap between receptive fields in V4 produces a population response, like that modeled by Pasupathy and Connor (2002), that is more discriminable for phase shifts of lower RF contours compared to phase shifts for higher RF contours. Indeed, equivalent phase shifts produce larger angular rotations of shape for low RF patterns, as seen in Fig. 5. Therefore, a decision making process monitoring the output of such a population code could make more acute judgments of phase for low versus high RF contours. Given such theories also predict that responses from curvature sensitive cells are integrated across curvature maxima (Dickinson et al., 2013; Dickinson et al., 2015; Dickinson et al., 2018; Habak et al., 2004; Poirier & Wilson, 2006), in Experiment 3 we investigate the importance of both maximum and minimum curvatures in contributing to effects of phase-dependent masking between shapes.

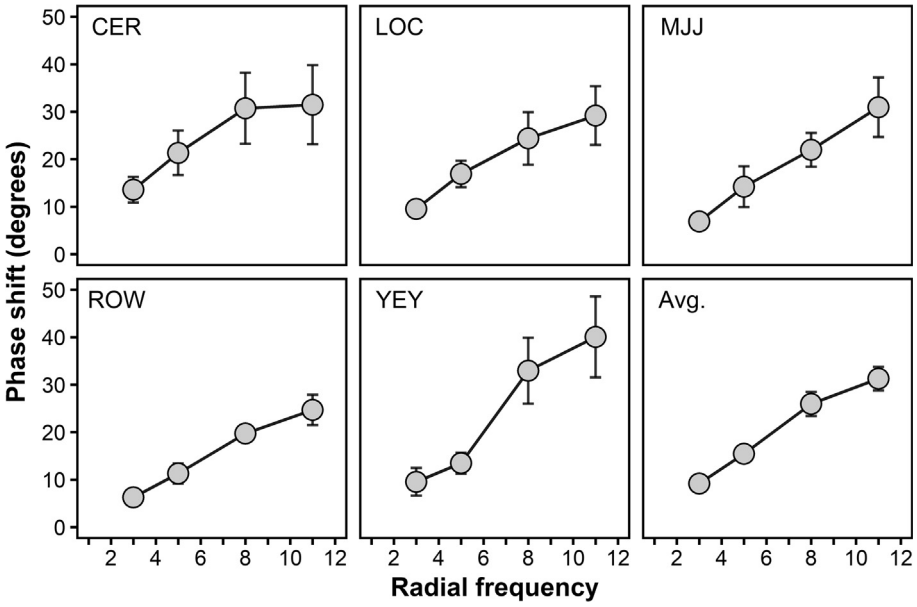


**Fig. 7.** For each observer, plot of thresholds for phase shifts (degrees) for single cycle contours of four radial frequencies. Error bars represent ± 1 SEM.

**Table 1**
Intercept, slope, and $R^2$ values of best-fitting line for each observer's data, and for average data, from Experiment 2.

| Observers | Intercept | Slope | $R^2$ |
|---|---|---|---|
| CER | 8.85 | 2.28 | 0.83 |
| LOC | 3.62 | 2.42 | 0.96 |
| MJJ | −1.38 | 2.95 | 0.99 |
| ROW | −0.34 | 2.34 | 0.98 |
| YEY | −3.92 | 4.14 | 0.94 |
| Mean | 1.37 | 2.82 | 0.94 |
| Median | −0.34 | 2.42 | 0.96 |
| Averaged | 1.37 | 2.82 | 0.97 |

## 3. Experiment 3: what contribution do maxima and minima of curvature have on phase dependent masking?

Models of shape perception often use the angular separation between curvature maxima and/or minima on closed-contour shapes to generate scale invariant representations of form (Dickinson et al., 2013; Dickinson et al., 2015; Dickinson et al., 2018; Pasupathy & Connor, 2001; Pasupathy & Connor, 2002; Poirier & Wilson, 2006). Furthermore, evidence from psychophysical studies suggest that the extent of alignment between curvature maxima (and minima) influences the magnitude of masking observed between two shapes (Habak et al., 2004; Habak et al., 2006; Habak et al., 2009; Poirier & Wilson, 2007). Experiment 3 therefore investigated the contribution of maxima and minima of curvature along a mask in modulating the effect of phase offset on masking strength that was observed in Experiment 1.

### 3.1. Methods

#### 3.1.1. Participants

Three young adults participated in Experiment 3 ($M$ = 23.33 years; $SD$ = 3.05). Observers MS and CR participated in Experiments 1 and 2, while observer AS was new to the study. Observer MS was the author, and observers AS and CR were naïve to the purpose of the experiment. All observers had normal or corrected-to-normal visual acuity. Experimental protocols were approved by the McMaster University Research Ethics Board, and consent of the participant was collected prior to the start of the experiment.

#### 3.1.2. Apparatus & stimuli

The apparatus was the same as the one used in Experiments 1 and 2, with mask amplitude set to 15× the baseline detection threshold for full cycle patterns. To isolate curvature extrema along masks, RF contours were positive or negative half-wave rectified yielding stimuli that contained only one kind of curvature feature (maxima or minima). Normal, unrectified RF contours were the same as those used in Experiment 1. The rectified contours contained positive and negative curvatures of unequal amplitude (i.e., stronger positive or negative component), whereas the full RF contour contained positive and negative curvatures of equal amplitude. It is important to note that half-wave rectified contours will contain curvatures of the opposite polarity at the junctions where a cycle rejoins the circular contour. For example, a convex half cycle will contain concavities on both sides of its deformation. This is a problem only if the operations that contribute to masking between shapes use unsigned curvature signals, as Max-Min extrema are perfectly aligned at 90° phase offset between half-wave rectified masks and full wave targets. However, we see improvements in thresholds moving from 0° to 90° phase offset between target and masks across all RF masking conditions (see Results section for Experiment 3), at least partially suggesting that curvature signals are encoded using a signed representation.

Examples of stimuli from Experiment 3 are shown in Fig. 8. A RF5

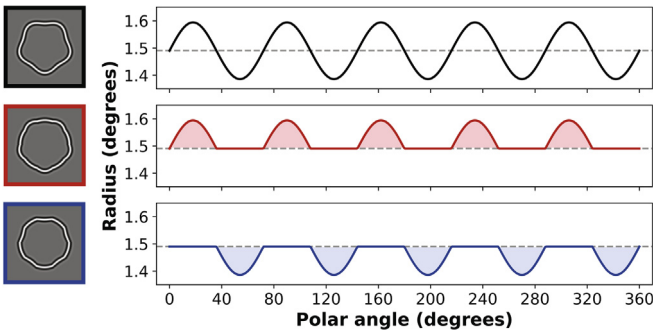


**Fig. 8.** Examples of full and half-wave rectified RF5 stimuli used in Experiment 3 (left panels) along with plots demonstrating how the radius changes as a function of polar angle (right panels). *Top:* Full wave RF5 contour. *Middle:* Positive half-wave rectified RF5 contour containing only positive curvature segments. *Bottom:* Negative half-wave rectified RF5 contour containing only negative curvature segments.

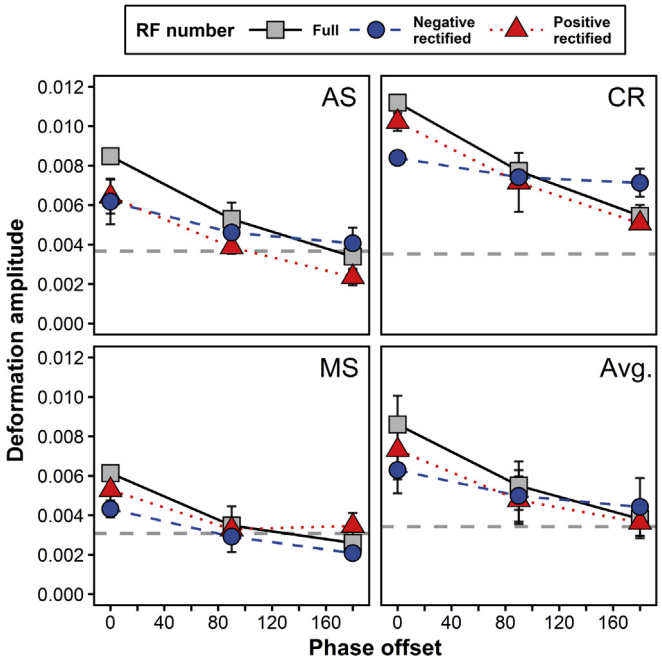


**Fig. 9.** Curvature detection thresholds measured in Experiment 3. Thresholds for full and half-wave rectified RF contours are represented by separate line types, and baseline thresholds are indicated by the horizontal dashed lines. Error bars represent ± 1 SEM.

contour was used because Experiment 1 found that the influence of phase was strongest at that radial frequency (Fig. 3).

#### 3.1.3. Procedure

The procedure was identical to that used in Experiment 1, except that target-mask phase offsets were restricted to only three values: 0°, 90°, and 180°.

### 3.2. Results

Fig. 9 displays detection thresholds for Experiment 3. When a target and mask were aligned in phase, thresholds were highest in the full contour condition, slightly lower in the condition in which masks contained only maximum (i.e., convex) curvature, and lowest in the condition where they contained only minimum (i.e., concave) curvatures. Performance was similar across conditions when target and masks were out of phase (i.e., phase offset = 180°).

Thresholds were analyzed with mixed linear models and the same corrective procedures used in the previous experiments. The model included two fixed effects (Curvature condition and Phase) and two random effects (Observer and Session). Quantitative analyses were consistent with observations described above: There were significant main effects of Curvature condition ($F_{2,45.08} = 4.74$, $p = .013$) and Phase ($F_{2,45} = 79.29$, $p < .0001$), and a significant Curvature condition × Phase interaction ($F_{4,45} = 5.70$, $p < .0001$).

Post-hoc comparisons between masking conditions were performed using paired, two-sided $t$ tests with $p$ values adjusted with the Holm-Bonferonni method and familywise $\alpha = 0.05$ (Holm, 1979). Comparisons were performed between curvature conditions at 0° phase, as this phase offset resulted in the greatest elevation in thresholds. The comparisons revealed significant differences between the full contour condition and both minimum ($p_{Holm} < .0001$) and maximum ($p_{Holm} = .0014$) curvature conditions. Also, there was a significant difference between maximum and minimum curvature conditions ($p_{Holm} = .014$).

#### 3.2.1. Discussion

Experiment 3 found that the effect of target-mask phase offset on detection thresholds varied across curvature conditions. The effect of the mask was greatest when its contour contained both maximum and minimum curvatures, and its effect was smaller when only maximum curvatures were present, and even smaller when only minimum curvatures were present. Furthermore, in all curvature conditions, detection thresholds were highest when the target and mask were phase aligned (0°) and declined monotonically with increasing phase offset. These results are consistent with previous work showing that masking between RF contours is driven primarily by the alignment of curvature maxima between neighbouring contours (Habak et al., 2004; Poirier & Wilson, 2006; Poirier & Wilson, 2007). Inspection of Fig. 9 shows that masking in the phase-aligned condition was greater for mask contours that contained curvature maxima rather than curvature minima, but masking was greatest when the mask contour contained both curvature maxima and minima. These results are inconsistent with previous suggestions that masking between contours is *exclusively* a consequence of alignments of curvature maxima (Habak et al., 2004; Poirier & Wilson, 2006). However these findings are consistent with a model of RF detection whereby observers detect curvature based on the difference between points of maximum and minimum extrema around a shape, as less masking is observed when this cue differs between the mask and target contours [i.e., less masking in half-wave rectified conditions](Schmidtmann & Kingdom, 2017). Overall, these results demonstrate the albeit weaker contribution of curvature minima to the effect of a mask on curvature detection thresholds.

## 4. General discussion

These experiments examined how phase alignment affects the magnitude of interaction between two shapes. Results from Experiments 1 and 3 replicate previous work demonstrating that masking is at its peak when two shapes are phase aligned, and declines monotonically with increasing phase offset between shapes. Experiment 1 extends these results by showing that masking was (approximately) a linear function of the phase offset that, surprisingly, did not differ across radial frequency. Experiment 2 found that phase discrimination was best for low RF contours, with thresholds increasingly monotonically with radial frequency. Lastly, Experiment 3 demonstrated that alignments of *both* curvature maxima and minima contribute to phase dependent masking between RF contours, although curvature maxima contribute more to the strength of masking than do curvature minima.

Together, these results suggest that curvature frequency does not affect the strength of phase-dependent masking between shapes, but does influence observers' ability to discriminate phase shifts of single-cycle shapes. In the following section, we interpret these results in relation to theories of masking based on the organization of curvature sensitive cells in visual cortex, as well as consider alternative ideas where phase dependent interactions arise upstream from mechanisms that integrate curvature across closed-contours.

### 4.1. Shape masking and local orientation filters

Models of shape perception attribute interactions between shapes to two main factors: the parallel alignment of contour segments (Hess et al., 1999; Poirier & Wilson, 2007), and alignment of curvature maxima relative to the center of a shape (Habak et al., 2004; Poirier & Wilson, 2006; Poirier & Wilson, 2007). Shape masking arising from the parallel alignment of contour segments is hypothesized to originate in primary visual cortex via weak local inhibition between orientation selective filters (Poirier & Wilson, 2006; Poirier & Wilson, 2007). Inhibition between local, orientation-selective neurons results in reduced neural responses that encode local contour orientation, thus providing weaker signals to higher visual areas that integrate information to represent shape (Poirier & Wilson, 2007). If signal strength about local

orientation along a contour is diminished, then more signal (i.e., more curvature) will likely be required for an observer to accurately detect changes in curvature along a shape, because detecting changes in curvature requires integrating local orientation along a contour (Loffler et al., 2003; Schmidtmann et al., 2012).

However, local inhibition between orientation-selective filters likely contributes only weakly to masking between shapes (Habak et al., 2004; Poirier & Wilson, 2007). If masking between contours was mediated by orientation selective mechanisms in V1, then circular (RF0) masks should produce significant masking. This prediction arises from the fact that, at detection threshold, the orientation of contour curvature along target shapes is more parallel to a circular mask than a curvature-modulated mask. However, previous work examining the effect of different RF masks on detection thresholds shows that circular masks cause little to no masking (Habak et al., 2004). Within the context of our study, this failure to see significant RF0 masking suggests that the decline in masking observed with increasing target-mask phase offset seen in Experiments 1 and 3 is only partially attributable to the divergent orientation structure accompanying phase misalignments between shapes. Instead, models of shape perception attribute interactions between shapes to largely be a consequence of the organization of curvature sensitive cells in V4 (Habak et al., 2004; Poirier & Wilson, 2006; Poirier & Wilson, 2007).

### 4.2. Phase dependent masking and alignment of curvature maxima

Several investigators have proposed that intermediate visual areas represent object outlines using a sparse coding scheme based on the angular separation between curvature maxima relative to the object center (Cadieu et al., 2007; Dickinson et al., 2013; Dickinson et al., 2015; Dickinson et al., 2018; Schmidtmann, Jennings, & Kingdom, 2015). Physiological data on the response properties of V4 neurons provides support for this polar-based coding scheme, as V4 neurons respond to curvature extrema relative to the center of a visual stimulus (Pasupathy & Connor, 2001; Pasupathy & Connor, 2002). The radial organization of V4 neurons allows for a scale invariant representation of shape, but it potentially could contribute to masking by concentric closed contour figures: if curvature extrema in the concentric contours occur at the same polar angle relative to the center of a shapes, then the response of neurons may saturate, resulting in an impaired ability to encode changes in curvature. Visual masking studies have shown that greater masking is produced by two masks than one (Habak et al., 2004), which is consistent with the idea that the responses of V4 curvature sensitive neurons may increase as more curvature features fall within their receptive fields. Habak et al., 2004 suggested that the response of curvature sensitive cells follow a compressive non-linear function with increasing number of curvature maximums falling in its receptive field. This non-linear response function implies that, as the mean response increases, a greater change in contour curvature will be required to produce a just noticeable change in the neuron's response. If observers use the responses of these V4 neurons to discriminate contour curvature, then thresholds will increase when a target contour is surrounded by a curved contour mask (Habak et al., 2004).

In the framework proposed by Habak et al. (2004), phase-dependent masking is a consequence of curvature maxima falling within the same receptive fields of curvature sensitive neurons (see Fig. 10). The results from Experiments 1 and 3 are consistent with this idea: As the phase offset between two shapes increases, curvature maxima will increasingly fall within non-overlapping receptive fields, thereby reducing the response of curvature selective neurons. This reduction in response will, in turn, reduce the amount of curvature that is needed to detect a change in the target's curvature. In other words, curvature detection thresholds should be greatest when the target and mask are phase aligned and decline as the phase offset increases, which is consistent the results we obtained in Experiments 1 and 3 (see Figs. 3 & 9).

Although excess pooling of contour curvature in V4 neurons explains why masking declines at greater target-mask phase offsets, it fails to explain why the effect of phase on thresholds is similar across RFs (Fig. 3). The absolute change in polar angle produced by a constant phase shift decreases as radial frequency increases (see Fig. 5). In other words, shifting curvature features (e.g., curvature maxima) by a specific polar angle requires a larger phase shift at high RFs than low RFs. If masking between shapes is entirely a consequence of excess spatial pooling of curvature features by V4 neurons, then smaller phase offsets should be required to significantly reduce masking in RF3 contours than RF11 contours unless, of course, the amount of excess/improper spatial pooling depends on *angle*, not *phase*. Contrary to this prediction, we found that the effect of phase offset on masking was similar across radial frequencies.

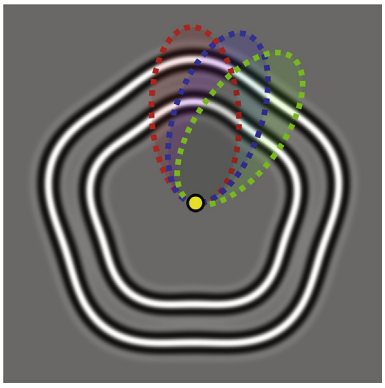

**Fig. 10.** Example of receptive fields of curvature sensitive neurons, such as those in V4, organized relative to the center of a RF5 contour.

A possible explanation for our failure to find an effect of RF on phase-selective masking is that the effect of phase on masking between shapes occurs after the stage where local curvature signals are combined. Poirier and Wilson (2006) developed a biologically plausible model for RF detection whereby the output of intermediary curvature detectors are cross-correlated with patterns of activity for different shapes (e.g., sine-wave like) stored in memory. This process is akin to the visual system performing a Fourier-like decomposition of curvature frequency along a contour, and was computationally implemented as a Fourier transform by Poirier and Wilson, 2006. Perhaps the similarity between curvature frequencies of a target and mask are judged based upon the output of a process akin to computing the dot product between two vectors encoding shape. The output of such a process would be the same across RF conditions with shifts in phase, despite the absolute shift in polar angle with changing phase differing as a function of radial frequency. These predictions also are consistent with previous studies arguing for the existence of shape channels, whereby different frequencies of curvature are encoded by channels sensitive to frequencies between approximately 3–10 cycles/$2\pi$ (Bell, Badcock, Wilson, & Wilkinson, 2007; Bell & Badcock, 2009; Bell et al., 2009; Habak et al., 2004).

One argument against this idea is that even when shapes are phase aligned, if the distance between two identical shapes is great enough, no masking is observed (Habak et al., 2004). This is one reason for arguing that masking between shapes is a consequence of curvature maxima falling within the same receptive fields of V4 neurons (Habak et al., 2004). In a study using stimuli formed by strings of Gabors arranged along one of several RF contours presented at different radial distances, Schmidtmann, Gordon, Bennett, and Loffler (2013) found that observers required fewer Gabors to detect modulated RF contours in noise when those Gabors were positioned along annuli of the same radius. Schmidtmann et al., 2013 argued that these results provide evidence for the existence of shape-specific analyzers that integrate orientation and position of local curvatures within individual annuli. Therefore, increasing the distance between shapes may result in a

decline in masking because fewer curvature features (e.g., maxima and minima) are falling within the same V4 receptive field, and this may result in shapes being processed by separate shape analyzers.

Overall, our results from Experiment 1 are consistent with arguments based upon the existence of shape channels, suggesting that phase-dependent masking may arise *following* processes that integrate curvature around closed contour shapes.

### 4.3. Sensitivity to shifts in phase of curvature features

Experiment 2 found that sensitivity to phase shifts between contours varies with radial frequency: Observers were more sensitive to phase for low RF single cycle contours compared to higher RF single cycle contours (Fig. 7). This increased sensitivity to phase is not the result of differences in curvature sensitivity across radial frequencies, as stimuli were presented at a constant multiple above detection threshold and, furthermore, the detection of contour curvature is phase (i.e., rotation) invariant (Bell & Badcock, 2009).

Another possible explanation is that the differences in sensitivity to phase result from the existence of multiple phase dependent channels whose tuning parameters differ across RF contours. Analogous to phase dependent masking, perhaps the ability to discriminate relative shifts in phase of shape relies upon a process that computes the similarity between stored representations of shape (i.e., shape channels), and the current shape being viewed. Because local curvature along low RF contours and internal representations of shape of similar frequency will be highly correlated despite changes in polar angle, such theories predict that larger angular rotations will be required for low RF contours to produce a just noticeable change in shape orientation as compared to high RF contours. In other words, such a theory predicts that phase sensitivity should remain the same across radial frequencies. However, such predictions are inconsistent with the results obtained in Experiment 2, that show observers' sensitivity to phase varying across radial frequency. Furthermore, it is unclear how this coding scheme would apply to shapes that contain large discontinuities in curvature along their contours (i.e., vertices), as such curvatures would contain power at extremely (infinitely) high frequencies.

Instead, differences in sensitivity to phase across RF contours may be a consequence of the population code used to encode shape. Behavioural data suggests that mechanisms used to code for shape identity might use a sparse representation based on angular positions of points of maximum curvature rather than dense representations based on the entire curvature around a shape (Dickinson et al., 2013; Dickinson et al., 2015; Dickinson et al., 2018). Such a sparse encoding scheme is supported by physiological evidence that suggests outline of shapes are represented by the peak response from a population of neurons selectively tuned to both curvature and position (Carlson, Rasquinha, Zhang, & Connor, 2011; Pasupathy & Connor, 2001; Pasupathy & Connor, 2002). In Experiment 2, curvature of single cycles of modulation differed as a function of the radial frequency from which they were sampled. Therefore, a population response of neurons sensitive to both curvature magnitude and position (i.e., polar angle), such as those in V4 (Carlson et al., 2011; Pasupathy & Connor, 2001; Pasupathy & Connor, 2002), will differ across RF contours even in the absence of shifts in phase of shape. Cycles of modulation sampled from low RF contours will have a large spatial spread, and thus elicit responses from neurons across many different polar angles. In contrast, curvature cycles sampled from high RF contours will elicit responses from neurons encoding a smaller range of polar angles. If the difference in population response evoked by shifts in phase is less informative for cycles of modulation sampled from certain RF contours compared to others, then the uniform effect of phase on masking may simply reflect this difference in sensitivity.

To test these predictions, and to better understand what information may be used by V4 to detect shifts of single cycle patterns from neural population codes, we developed a computational model that is similar to the one described by Pasupathy and Connor (2002). The model, described in the following section, uses patterns of activation from neural population codes as a tool for formulating and evaluating linking propositions between behavioural data and the neurophysiology of shape perception. We briefly describe each stage of the model below, and emphasize that the simulation results that follow are not especially sensitive to minor changes in the values of hyperparameters chosen at each stage of the model.

#### 4.3.1. Computational model of V4: methods

The first stage of the model translates a shape from 2-dimensional Cartesian coordinates to polar coordinates by encoding the angular position and degree of radial modulation of the closed contour shape relative to object center. This stage is consistent with both behavioural (Habak et al., 2004; Wilkinson et al., 1998) and physiological (Pasupathy & Connor, 2001; Pasupathy & Connor, 2002) evidence that suggests cortical areas along the ventral visual pathway may encode closed contour forms using such an encoding scheme.

The second stage of the model represents curvature ($c$), here defined as the rate of change in tangent angle with respect circular. We chose to use this definition of curvature, as this was the definition adopted in the model developed by (Poirier & Wilson, 2006), and was subsequently used by authors studying RF detection and discrimination (Dickinson et al., 2013; Dickinson et al., 2015; Dickinson et al., 2018). For an alternative definition of curvature, see Schmidtmann and Kingdom (2017). Thus, we computed curvature as the second derivative of the contour's modulation amplitude, $A$, with respect to the shape radius ($r$) and polar angle, $\theta$:

$$c_\theta = \frac{r^2 A_\theta}{r\theta} \tag{6}$$

Eq. (6) cannot be solved analytically for single-cycle contours, and therefore we estimate curvature numerically using central difference differentiation.

Because abrupt changes in orientation (e.g., vertices) can result in discontinuities in otherwise smooth curvature functions, in Stage 3 the absolute curvature ($c$) at each point along the contour is replaced with a $c'$ to mirror the measure used by Pasupathy and Connor (2001, 2002):

$$c'_\theta = \frac{1}{1 + \exp^{-\alpha c_\theta}} \tag{7}$$

Eq. (7) is a sigmoidal function that ensures all curvature values along the contour are mapped onto values that range between $-1$ (strongly concave) to $+1$ (strongly convex). Parameter $\alpha$, which controls the slope of the sigmoidal function, was set to 2 for our simulations because this value ensures that radial modulation amplitudes for the patterns in our experiments would elicit fairly strong responses from the neural population.

In the fourth stage of the model, values of $c'$ are sampled at $P$ equally-spaced points along the contour. In our simulations, $P$ was set to an arbitrary value of 30, which was adequate for the contours used in our experiments. Changing $P$ did not alter our key results except for low values that sparsely sample the $c'$ function (i.e., $P < 8$).

Each curvature-sensitive unit (i.e., V4 neuron) responds to two stimulus parameters: position in polar angle ($\theta$) and curvature ($c'$). In the fifth stage of the model, the response of each unit is modelled as a 2-dimensional Gaussian function defined by Eq. (8):

$$a_{map}(\theta, c') = \frac{1}{2\pi\sigma_\theta\sigma_{c'}} e^{-[((\theta-\mu_\theta)^2/2\sigma_\theta^2)+((c'-\mu_{c'})^2/2\sigma_{c'}^2)]} \tag{8}$$

The shape of each 2-D Gaussian function for each unit was controlled by values of $\mu$ and $\sigma$, where $\mu$ determines the location of peak response (i.e., maximal activation) for the tuning function along the dimension under examination, and $\sigma$ determines the spread of this function. We chose to model parameters that closely resembled that of Pasupathy and Connor (2002). Thus, the value of $\sigma$ for angular position and

curvature was 25° and 0.125, respectively.

In Stage 6, the overall response of a unit to a sampled stimulus with $P$ points was set to equal the maximum response recorded for that unit in response to each point in $P$. This procedure is similar to that used by (Pasupathy & Connor, 2001), whereby the response $r$ of a single unit is given by:

$$r(\theta, c') = \max_P[a_{map}(\theta, c')] \tag{9}$$

The response of each unit will be strong if its preferred features are present within a shape, and will grade its response accordingly if those features deviate from this preferred combination of features.

In Stage 7, the response of each unit was scaled by a sigmoidal function that attenuated the response from units whose preferred curvature lies proximate to, or at zero. The function was defined as:

$$r_{weighted}(\theta, c') = \frac{1}{1 + e^{-a \cdot |c'|}} \cdot r(\theta, c') \tag{10}$$

where $a$ determines the slope of the function, and was set to a value of 2.5, which provides a modest attenuation of the response from units that prefer zero curvature. Applying such an attenuation to unit responses near zero curvature makes circularity a neural default, and is consistent with previous models of V4 (Carlson et al., 2011; Habak et al., 2004; Wilkinson et al., 1998).

In Stage 8, we defined how many units $N$ to model, which determines the density at which the feature space (defined by $\theta$ and $c'$) is sampled. In total, 900 units were modelled that uniformly represented curvature across all angular positions, and approximated the number of units used by Pasupathy and Connor (2002).

Finally, responses at each combination of $\theta$ and $c'$ are summed and normalized across all units:

$$S = p_{map}(\theta, c') = \frac{\sum_{k=1}^{N} r_{weighted}(\theta, c')}{\max[r_{weighted}(\theta, c')]} \tag{11}$$

The final population response represented by matrix $S$ is a surface that encodes changes in curvature along the contour of a shape at different polar angles.

#### 4.3.2. Computational model of V4: simulations

In total, eight simulations were run. Each single-cycle contour in Experiment 2 was run through the computational model to produce a response surface, where peaks along the surface represent maximal divergence in curvature (positive or negative) from circularity. Each contour was then rotated in polar angle by 3° and was once again run through the model to produce a new population response. A 3° angle of rotation was chosen because this value is roughly equivalent to the minimum phase shift that could be detected for each single cycle contour tested in Experiment 2. Therefore, this angular rotation (i.e., differing phase shift across RF) would be especially diagnostic in understanding what factors limit the ability of observers in detecting shifts in phase of shape that contain different degrees of curvature along their contour. The difference in population response elicited from the presentation of each contour at a phase shift that was at threshold for human observers, as measured in Experiment 2, was then computed to examine what information may be available to the visual system to use to compute differences in shifts in phase across shapes.

#### 4.3.3. Computational model of V4: results

Results from the simulations are displayed in Fig. 11. Examination of the population surfaces on the left on the figure demonstrates all three single-cycle contours elicit strong responses from curvature sensitive units, with the strength of activation of units identifying the presence of curvature extrema across polar angles. Restricting our examination along the curvature dimension also demonstrates that regions of peak activation for curvature extrema occur closer in feature space for low frequency single-cycle contours compared to contours sampled from higher frequency contours. Furthermore, the low-frequency contour elicits a broad pattern of activation across units, while intermediate and higher frequency shapes elicit more localized response patterns. Population surfaces generated by our model to shapes of different contour curvatures are consistent with the types of population responses to shape produced by Pasupathy and Connor (2001)'s model of V4 neurons.

Despite a small angular rotation of 3° applied to each shape, the resultant population response was similar, but not identical, in units representing each version of the same shape at different polar angles. The difference map highlights what information may be utilized by the visual system in using such an encoding scheme to detect shifts in phase of shape. To quantify the similarity of population surfaces between phase shifted patterns, we computed the Mean-squared error (MSE) between activation maps generated by our model, as outlined in Table 2. Smaller MSEs suggest the surface maps are more similar, while larger MSEs suggest that surface maps are less similar. For the single-cycle RF3 contours, the population responses were very similar, resulting in a nearly flat difference map. These results suggest that the visual system may be utilizing sources of information besides curvature, or using a different scheme to encode curvature, to detect rotations of shapes that contain low-frequency curvatures. In contrast to low-frequency contours, difference maps generated for intermediate and high frequency contours contain noticeable differences in localized regions along the response surface. Therefore, information exists along the population surface that would allow the visual system to accurately discriminate rotations of these shapes. This result suggests that although such an encoding scheme can be used by the visual system in making such rotational judgments of shape that contain higher magnitudes of curvature, it is likely that other factors, such as noise introduced at various stages along visual processing, or spatial uncertainty may be responsible for limiting perception in these circumstances. In Experiment 2, observers were more sensitive to shifts in phase of shape for low curvature contours compared to high curvature. Stated differently, sensitivity to angular rotation was roughly the same across RF contours. Given the difference map for the intermediate and high frequency sampled shapes both contain useful information in making a judgment as to whether the shape was phase shifted, why are thresholds for higher frequency shapes similar to that of the low frequency shape in Experiment 2? If performance at discriminating shifts in phase was correlated with the visual system detecting any difference in activity between population responses, then thresholds for detecting shifts in phase should be similar or *lower* for the high curvature shape compared to others tested. One possibility is that the population response generated in areas such as V4 is not the limiting factor in discriminating shifts in phase for shapes of different curvature. Perhaps, the visual system does not rely upon use of such representations to code for phase of shapes, or that curvature signals are altered at lower visual areas that further complicates the mapping of curvature signals onto a distributed population surface using such an encoding scheme.

An alternative explanation is that thresholds for the high frequency shape are similar to that for the low frequency shape because of the effects of spatial uncertainty on locating peaks of curvature for the single-cycle RF11 contour. Difference maps generated by our model for intermediate and high frequency sampled shapes contain diagnostic information to make judgments about the rotation of a shape. Therefore, what may be limiting performance in phase discrimination of shape at high radial frequencies may be the ability in coding the position of curvature extrema at specific polar angles. Such arguments are not immediately captured by the response properties of neurons in V4, as shown by our simulations. One way to make the difference maps more similar across RF contours in the model is by making the spread of the tuning curve that responds to location (i.e., polar angle), which corresponds to $\sigma$ in Eq. (8), increase as a linear function of radial frequency. This would have an overall effect of introducing more noise in

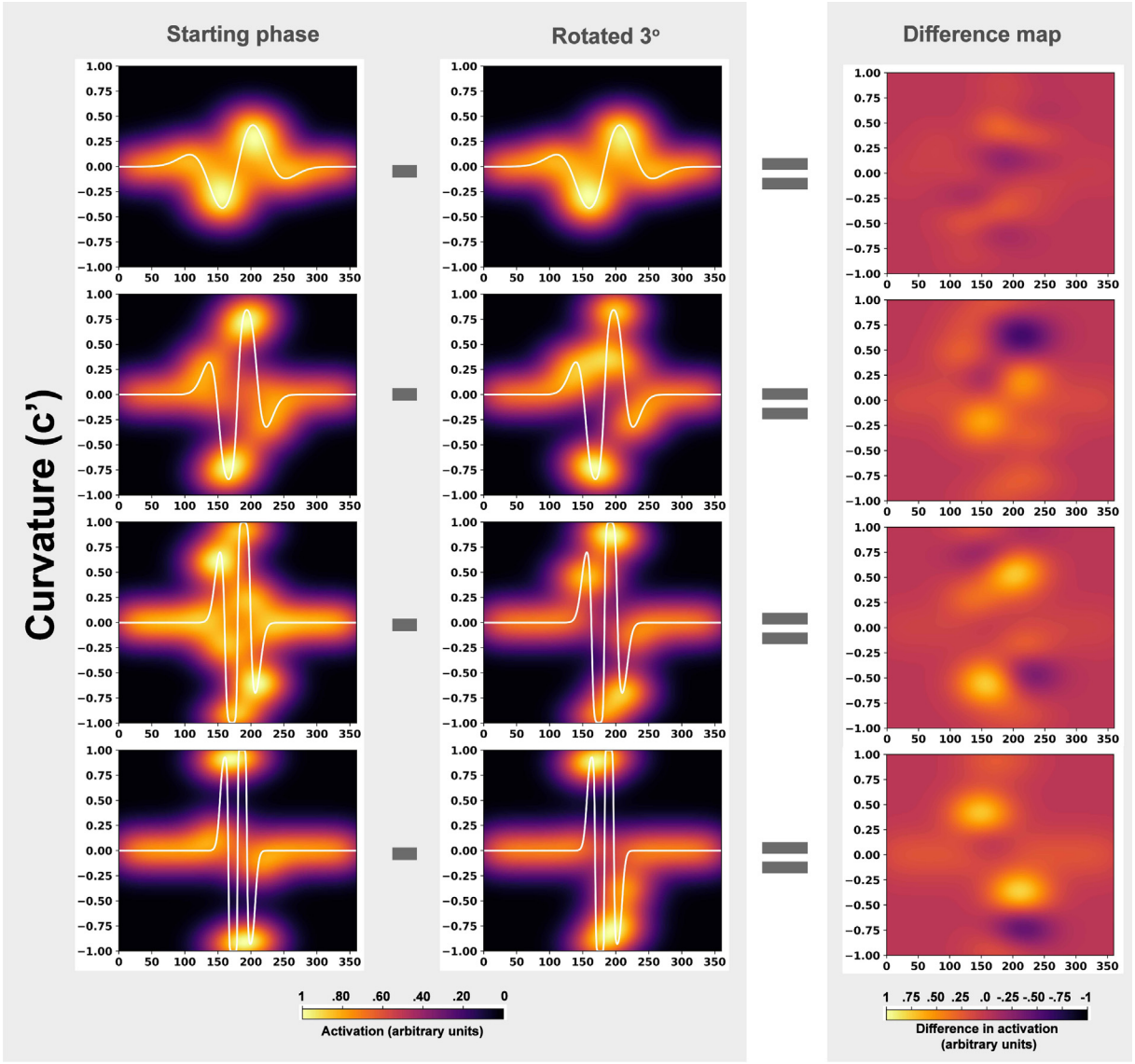


**Fig. 11.** *Left & Middle columns:*. Simulated population responses to contours used in Experiment 2. Unit activation ranged from 0 (black) to 1 (yellow). In each panel, the ordinate represents curvature, ranging from −1 (sharp concave) to 1 (sharply convex), and the abscissa represents angular position along the contour. The RF3, RF5, RF8, and RF11 contours used in Experiment 2 were used in all simulations: they are displayed in the bottom-left corner of each panel in the left column, and as white lines ($c'$ mapping) in the left and middle columns. Responses were calculated for each RF at an initial angle of rotation and again after rotating the shape by 3°. The population surfaces generated did a good job at capturing curvature extrema, and more general curvature features across all polar angles. *Right column:* Difference maps produced by subtracting the response surfaces.

**Table 2**
Mean-squared error between activation surface maps generated by our V4 model when presented with a single-cycle RF contour, and the same contour shifted by 3° of angular rotation. Smaller MSEs suggest the surface maps are more similar, while larger MSEs suggest that surface maps are less similar.

| Single-cycle RF number | Mean-squared Error (MSE) |
|---|---|
| RF3 | 0.018 |
| RF5 | 0.029 |
| RF8 | 0.034 |
| RF11 | 0.036 |

coding for location of curvatures depending on curvature frequency, and would help account for our results from Experiment 2. However, it is unclear whether spatial uncertainty arises as a result of changes in the properties of tuning functions that respond to curvatures at the level of V4, or whether this uncertainty may arise elsewhere in the visual system. Therefore, future work should aim to elucidate how spatial uncertainty may effect the population response of neurons in V4 at encoding properties of shape.

#### 4.3.4. Computational model of V4: comparison with other models

Many computational models of shape currently exist (Carlson et al., 2011; Hatori, Mashita, & Sakai, 2016; Kempgens, Loffler, & Orbach, 2013; Pasupathy & Connor, 2001; Pasupathy & Connor, 2002; Poirier & Wilson, 2006; Poirier & Wilson, 2010; Schmidtmann et al., 2015; Schmidtmann & Kingdom, 2017). These models, as well as the one described here, build on the seminal work of Pasupathy and Connor (2001, 2002) suggesting that shape is encoded using a population surface that represents curvature at different polar angles.

Although the models differ significantly in their details, they all assume that neural response rates increase with the rate of curvature change, and the sparseness of the resulting representations depends on the gain of the response function. Hatori et al. (2016) demonstrated that by explicitly enforcing a penalty in their model to produce medium degrees of sparseness, curvature selectively and bias was produced in the population activity of units that resembled V4 neurons. Slugocki et al. (2018) have also shown that sparse representational vectors of shape can be used by machine learning agents to learn simple shape identities, which suggests that not all curvature information is pertinent to encoding identity. Attneave (1954) was one of the first to suggest not all information encoded carries equal perceptual weighting; an idea inspired by information theory.

We expect that models that use a population code to represent curvatures (Carlson et al., 2011; Kempgens et al., 2013; Pasupathy & Connor, 2001; Pasupathy & Connor, 2002; Poirier & Wilson, 2006), will be able to account for the effects of phase presented here. Specifically, the ability of a decision process analyzing these population responses to discriminate shifts in phase of shapes should be limited by the resolution at which the angular positions of curvature extrema are coded. However, our model implemented only a minor sparseness constraint in coding for curvature (i.e., Stage 7), and therefore the resultant population surface is able to capture more subtle differences in shifts in phase between two shapes. In contrast, models that enforce strong sparseness constraints (e.g., Carlson et al., 2011; Hatori et al., 2016) should require larger phase shifts to differentiate between complex shapes. Because extremely sparse coding schemes lose information about curvature occurring between curvature extrema, changes in the population response for these points cannot be used to judge shifts in phase between shapes. Thus, future work should examine how sparseness affects the ability of computational models to discriminate phase-shifted shapes of varying contour complexity. Furthermore, it would be interesting to investigate how other models of shape that do not rely upon position coding of curvature, such as Schmidtmann and Kingdom (2017), might predict human phase discrimination.

### 4.4. Importance of curvature extrema in masking between shapes

Masking studies using RF contours attribute the interaction between shapes to be primarily the consequence of the alignment of curvature maxima (Habak et al., 2004; Habak et al., 2006; Habak et al., 2009; Poirier & Wilson, 2007), with little mention with regards to the contribution of curvature minima. Such theories of shape masking are also consistent with models of RF detection that claim only points of maximum curvature are used to code for shape identity (Poirier & Wilson, 2006). Contrary to previous work, results from Experiment 3 demonstrate that the alignment of either curvature maxima or minima result in masking between two identical, phase aligned shapes, although the effect of masking was greatest when the mask that contained both curvature extrema. One argument against this idea is that half-wave rectified contours still contain curvatures of the opposite polarity where the cycle rejoins the circular portion of the shape, albeit occurring at smaller amplitudes than in full waveform counterparts, and therefore masking can still occur between these features and full cycles appearing in the target. However, such arguments also predict that peak masking for the negative half-wave rectified condition should occur when the phase offset between target and masks is at 90°, as positive full-cycles of the target would be in perfect alignment with the positive curvatures occurring at the transitional segments in masks. Contrary to this prediction, less masking was found for 90° phase offsets relative to the condition in which both target and negative half-wave rectified contours are in perfect alignment (i.e., 0°).

Consistent with the results of Experiment 3, physiological evidence suggests the use of population codes within V4 to encode shapes that operate along a continuum of features; namely curvature and angular position (Pasupathy & Connor, 2001; Pasupathy & Connor, 2002). Therefore, although phase dependent masking is hypothesized to primarily result from the excess summation of curvature signals within V4 receptive fields, this explanation need not be exclusive to peaks of curvature. Instead, data from Experiment 3 argue that alignment of curvature minima may also produce effects associated with excess summation of curvature signals within receptive fields tuned to curvature. Data from Experiment 3 are also consistent with psychophysical studies that suggest both curvature types contribute equally to the perception of global shape (Bell, Hancock, Kingdom, & Peirce, 2010; Kempgens et al., 2013; Schmidtmann et al., 2015; Schmidtmann & Kingdom, 2017).

Data from Experiment 3 also are consistent with the model proposed by Schmidtmann and Kingdom (2017) whereby RF contours are detected based on the difference between maximum and minimum curvatures. If observers use curvature differences to detect changes in modulation amplitude, perhaps this metric might also be used by the human visual system to judge the similarity between shapes. Following this line of reasoning, greater masking should be observed between shapes that share a similar difference in curvature between Max-Min points. Therefore, less masking should be observed between a full-wave target and half-wave rectified masks in comparison to masks that contain a full waveform. Our data from Experiment 3 are consistent with such a model of curvature detection: less masking was observed in conditions where the Max-Min difference between targets and masks differed as a result of applying a half-wave rectification to masking contours. Future work should aim to extend the mathematical reasoning of this model to explicitly predict masking effects between shapes, and how phase-dependent masking might emerge using a difference score between Max-Min curvatures.

### 4.5. Conclusion

To summarize, we demonstrated that the effect of phase on masking between shapes does not differ across radial frequencies. However, sensitivity at discriminating shifts in phase does differ as a function of radial frequency, and helps to explain the uniform effect of phase on masking across RF contours. Surprisingly, differences in sensitivity to phase are not captured by models of V4 neurons that produce population surfaces in response to the magnitude and position of curvature, and therefore alternative explanations are needed. Finally, using half-wave rectified masks, we showed that both curvature maxima and minima contribute to phase dependent masking between shapes based on angular alignment of these features relative to the origin of a shape.

## Acknowledgments

Financial support was provided by Discovery Grants to A.B. Sekuler and P.J. Bennett from the Natural Sciences and Engineering Research Council of Canada (NSERC).

## References

Alam, M., Vilankar, K. P., Field, D. J., & Chandler, D. M. (2014). Local masking in natural images: A database and analysis. *Journal of Vision, 14*(22), 1–38.
Altmann, C. F., Bülthoff, H. H., & Kourtzi, Z. (2003). Perceptual organization of local elements into global shapes in the human visual cortex. *Current Biology, 13*(4), 342–349.
Attneave, F. (1954). Some informational aspects of visual perception. *Psychological Review, 61*(3), 183–193.
Baldwin, A. S., Schmidtmann, G., Kingdom, F. A. A., & Hess, R. F. (2016). Rejecting probability summation for radial frequency patterns, not so Quick!. *Vision Research, 122*, 124–134.
Bates, D., Mächler, M., Bolker, B., & Walker, S. (2015). Fitting linear mixed-effects models using lme4. *Journal of Statistical Software, 67*(1), 1–48.
Bell, J., & Badcock, D. R. (2009). Narrow-band radial frequency shape channels revealed by sub-threshold summation. *Vision Research, 49*(8), 843–850.
Bell, J., Badcock, D. R., Wilson, H., & Wilkinson, F. (2007). Detection of shape in radial frequency contours: Independence of local and global form information. *Vision Research, 47*(11), 1518–1522.
Bell, J., Hancock, S., Kingdom, F. A. A., & Peirce, J. W. (2010). Global shape processing:

Which parts form the whole? *Journal of Vision, 10*(6), 16.
Bell, J., Wilkinson, F., Wilson, H. R., Loffler, G., & Badcock, D. R. (2009). Radial frequency adaptation reveals interacting contour shape channels. *Vision Research, 49*(18), 2306–2317.
Brainard, D. H. (1997). The psychophysics toolbox. *Spatial Vision, 10*, 433–436.
Cadieu, C., Kouh, M., Pasupathy, A., Connor, C. E., Riesenhuber, M., & Poggio, T. (2007). A model of V4 shape selectivity and invariance. *Journal of Neurophysiology, 98*(3), 1733–1750.
Carlson, E. T., Rasquinha, R. J., Zhang, K., & Connor, C. E. (2011). A sparse object coding scheme in area V4. *Current Biology, 21*(4), 288–293.
Day, M., & Loffler, G. (2009). The role of orientation and position in shape perception. *Journal of Vision, 9*(10) 14.1–17.
Dickinson, J. E., Bell, J., & Badcock, D. R. (2013). Near their thresholds for detection, shapes are discriminated by the angular separation of their corners. *PLoS ONE, 8*(5), 1–9.
Dickinson, J. E., Cribb, S. J., Riddell, H., & Badcock, D. R. (2015). Tolerance for local and global differences in the integration of shape information. *Journal of Vision, 15*(3), 21.
Dickinson, J. E., Haley, K., Bowden, V. K., & Badcock, D. R. (2018). Visual search reveals a critical component to shape. *Journal of Vision, 18*(2), 2.
Dickinson, J. E., McGinty, J., Webster, K. E., & Badcock, D. R. (2012). Further evidence that local cues to shape in RF patterns are integrated globally. *Journal of Vision, 12*(12), 16.
Geisler, W. S., Perry, J. S., Super, B. J., & Gallogly, D. P. (2001). Edge co-occurrence in natural images predicts contour grouping edge co-occurrence in natural images predicts contour grouping performance. *Vision Research, 41*(6), 711–724.
Green, R. J., Dickinson, J. E., & Badcock, D. R. (2017). Global processing of random-phase radial frequency patterns but not modulated lines. *Journal of Vision, 17*(9), 18.
Green, R. J., Dickinson, J. E., & Badcock, D. R. (2018c). Convergent evidence for global processing of shape. *Journal of Vision, 18*(7), 7.
Green, R. J., Dickinson, J. E., & Badcock, D. R. (2018a). The effect of spatiotemporal displacement on the integration of shape information. *Journal of Vision, 18*(5), 4.
Green, R. J., Dickinson, J. E., & Badcock, D. R. (2018b). Integration of shape information occurs around closed contours but not across them. *Journal of Vision, 18*(5), 6.
Habak, C., Wilkinson, F., & Wilson, H. R. (2006). Dynamics of shape interaction in human vision. *Vision Research, 46*(26), 4305–4320.
Habak, C., Wilkinson, F., & Wilson, H. R. (2009). Preservation of shape discrimination in aging. *Journal of Vision, 9*(12) 18.1–8.
Habak, C., Wilkinson, F., Zakher, B., & Wilson, H. R. (2004). Curvature population coding for complex shapes in human vision. *Vision Research, 44*(24), 2815–2823.
Hatori, Y., Mashita, T., & Sakai, K. (2016). Sparse coding generates curvature selectivity in V4 neurons. *JOSA A, 33*(4), 527–537.
Hess, R. F., Wang, Y. Z., & Dakin, S. C. (1999). Are judgements of circularity local or global? *Vision Research, 39*(26), 4354–4360.
Holm, S. (1979). A simple sequentially rejective multiple test procedure. *Scandinavian Journal of Statistics, 6*(3), 65–70.
Jeffrey, B. G., Wang, Y. Z., & Birch, E. E. (2002). Circular contour frequency in shape discrimination. *Vision Research, 42*(25), 2773–2779.
Judd, C. M., Westfall, J., & Kenny, D. A. (2012). Treating stimuli as a random factor in social psychology: A new and comprehensive solution to a pervasive but largely ignored problem. *Journal of Personality and Social Psychology, 103*(1), 54–69.
Kempgens, C., Loffler, G., & Orbach, H. S. (2013). Set-size effects for sampled shapes: Experiments and model. *Frontiers in Computational Neuroscience, 7*.
Kenward, M. G., & Roger, J. H. (1997). Small sample inference for fixed effects from restricted maximum likelihood. *Biometrics, 53*(3), 983–997.
Kurki, I., Saarinen, J., & Hyvarinen, A. (2014). Investigating shape perception by classification images. *Journal of Vision, 14*(12), 1–19.
Loffler, G., Wilson, H. R., & Wilkinson, F. (2003). Local and global contributions to shape discrimination. *Vision Research, 43*(5), 519–530.
Pasupathy, A., & Connor, C. E. (2001). Shape representation in area V4: Position-specific tuning for boundary conformation. *Journal of Neurophysiology, 86*(5), 2505–2519.
Pasupathy, A., & Connor, C. E. (2002). Population coding of shape in area V4. *Nature Neuroscience, 5*(12), 1332–1338.
Pelli, D. G. (1997). The videotoolbox software for visual psychophysocs: Transforming numbers into movies. *Spatial Vision, 10*, 437–442.
Poirier, F. J., & Wilson, H. R. (2006). A biologically plausible model of human radial frequency perception. *Vision Research, 46*(15), 2443–2455.
Poirier, F. J., & Wilson, H. R. (2007). Object perception and masking: Contributions of sides and convexities. *Vision Research, 47*(23), 3001–3011.
Poirier, F. J. A. M., & Wilson, H. R. (2010). A biologically plausible model of human shape symmetry perception. *Journal of Vision, 10*(1), 9.
R Core Team (2017). *R: A Language and Environment for Statistical Computing.* Vienna, Austria: R Foundation for Statistical Computing.
Schmidtmann, G., Gordon, G. E., Bennett, D. M., & Loffler, G. (2013). Detecting shapes in noise: Tuning characteristics of global shape mechanisms. *Frontiers in Computational Neuroscience, 7*.
Schmidtmann, G., Jennings, B. J., & Kingdom, F. A. A. (2015). Shape recognition: convexities, concavities and things in between. *Scientific Reports, 5*, 17142.
Schmidtmann, G., Kennedy, G. J., Orbach, H. S., & Loffler, G. (2012). Non-linear global pooling in the discrimination of circular and non-circular shapes. *Vision Research, 62*, 44–56.
Schmidtmann, G., & Kingdom, F. A. A. (2017). Nothing more than a pair of curvatures: A common mechanism for the detection of both radial and non-radial frequency patterns. *Vision Research, 134*, 18–25.
Slugocki M, Sekuler AB, Bennett PJ. Effect of signal alteration on learning shape identity using sparse representations. Conference on Cognitive Computational Neuroscience; 2018.
Wang, Y.-Z., & Hess, R. F. (2005). Contributions of local orientation and position features to shape integration. *Vision Research, 45*(11), 1375–1383.
Weibull, W. (1951). A statistical distribution function of wide applicability. *Journal of Applied Mechanics, 18*, 292–297.
Wilkinson, F., Wilson, H. R., & Habak, C. (1998). Detection and recognition of radial frequency patterns. *Vision Research, 38*(22), 3555–3568.
Wilson, H. R., & Wilkinson, F. (2002). Symmetry perception: A novel approach for biological shapes. *Vision Research, 42*(5), 589–597.
Wilson, H. R., Wilkinson, F., Lin, L. M., & Castillo, M. (2000). Perception of head orientation. *Vision Research, 40*(5), 459–472.